Transesterification of Dimethyl Oxalate with Phenol Over TiO_2/SiO_2: Catalyst Screening and Reaction Optimization

Xia Yang
Key Laboratory for Green Chemical Technology, School of Chemical Engineering and Technology, Tianjin University, Tianjin 300072, China, and
School of Chemical and Biomedical Engineering, Nanyang Technological University, Singapore 637459, Singapore

Xinbin Ma and Shengping Wang
Key Laboratory for Green Chemical Technology, School of Chemical Engineering and Technology, Tianjin University, Tianjin 300072, China

Jinlong Gong
Key Laboratory for Green Chemical Technology, School of Chemical Engineering and Technology, Tianjin University, Tianjin 300072, China, and
Dept. of Chemical Engineering, University of Texas at Austin, Austin, TX 78712

DOI 10.1002/aic.11613
Published online October 29, 2008 in Wiley InterScience (www.interscience.wiley.com).

Physicochemical properties of silica-supported titanium oxide catalysts as well as their performances for transesterification of dimethyl oxalate (DMO) with phenol to methyl phenyl oxalate (MPO) and diphenyl oxalate (DPO) have been investigated systematically. Various wt % of TiO_2 were loaded on SiO_2 by a two-step wet impregnation method. The surface properties of TiO_2/SiO_2 catalysts were explored by various characterization techniques (BET, SEM, ICP, XPS, XRD, FTIR of pyridine adsorption, and NH_3-TPD). Catalytic performances of TiO_2/SiO_2 catalysts were found to be strongly dependent on TiO_2 dispersion and surface acidity. Monolayer dispersion capacity of TiO_2 on silica was estimated to be about 4.0 TiO_2 molecules per nm^2 (SiO_2) and no crystalline TiO_2 was detected at TiO_2 loading less than 12 wt %. FTIR and TPD analysis suggested that weak Lewis acid sites on the surface of TiO_2/SiO_2 were responsible for their unique selectivity to the target products, MPO and DPO. An optimization of reaction conditions for the transesterification of DMO with phenol was performed over 12 wt % TiO_2/SiO_2 calcined at 550°C. In addition, we studied the disproportionation reaction from MPO to DPO via a catalytic distillation process, which is highly efficient to promote formation of the desired DPO. *AIChE J*, 54: 3260–3272, 2008
Keywords: diphenyl carbonate, diphenyl oxalate, methyl phenyl oxalate, transesterification, TiO_2/SiO_2, monolayer, acid sites, disproportionation

Correspondence concerning this article should be addressed to X. Ma at xbma@tju.edu.cn.

Introduction

Aromatic polycarbonates (PCs) are excellent engineering thermoplastics and substitutes for metals and glass because

of their excellent optical and electrical properties, high impact strength, thermal resistance, and transparency.[1–3] Currently, the annual worldwide production of PCs is more than 1.5 million tons, and consumption and applications of PCs are growing stably.[4] With increasing demands for environmentally friendly or "Green" processes for PCs synthesis, considerable efforts have been made to improve or to essentially replace the conventional phosgene method, where highly toxic phosgene is used as the reagent with copious amounts of methylene chloride as the solvent. One of the important commercial processes for PCs synthesis is the transesterification of 2,2-bis (4-hydroxyphenol)propane (bisphenol A) with diphenyl carbonate (DPC).[5] This non-phosgene method has distinct environmental and economic advantages. As an important precursor for PCs production, DPC and its synthesis have received great attention. Several methods, including oxidative carbonylation of phenol and transesterification reactions, have been reported and developed for DPC synthesis.[6–12] Among them, a three-step reaction, consisting of preparation of dimethyl oxalate (DMO), transesterification of DMO with phenol to produce diphenyl oxalate (DPO), followed by decarbonylation of DPO to DPC (as shown in reactions 1–3) has been proposed. This process is environmentally feasible from avoiding the use of toxic or corrosive reagents. Furthermore, methanol and CO produced in both reactions 2 and 3 can be easily separated from the system, and reused in the reaction 1. Thus, this route is attracting great interests because of its green technology and high atom economy.[13–15]

$$2CO + 2MeOH + 1/2O_2 \rightleftharpoons MeOCCOMe + H_2O \quad (1)$$

(DMO)

$$MeOCCOMe + 2PhOH \rightleftharpoons PhOCCOPh + 2MeOH \quad (2)$$

(DMO) (DPO)

$$PhOCCOPh \rightleftharpoons PhOCOPh + CO \quad (3)$$

(DPO) (DPC)

The preparation of DMO by oxidative carbonylation of methanol (reaction 1) has been commercialized.[16] Based on our previous study,[17] decarbonylation of DPO to DPC (reaction 3) can be easily implemented over a Ph_4PCl catalyst, giving 99.5% DPO conversion with 98.3% DPC selectivity. Therefore, synthesis of DPO from the transesterification of DMO with phenol as shown in reaction 2 is the key process due to the low thermodynamic equilibrium constant (1.1×10^{-8} at 180°C).[17] Herein, the synthesis of DPO is performed in two steps: formation of methyl phenyl oxalate (MPO) and further disproportionation of MPO to DPO, as shown reactions 4 and 5.

$$MeOCCOMe + PhOH \rightleftharpoons PhOCCOMe + MeOH \quad (4)$$

(DMO) (MPO)

$$2\,PhOCCOMe \rightleftharpoons PhOCCOPh + MeOCCOMe \quad (5)$$

(MPO) (DPO) (DMO)

Homogeneous catalytic systems such as Lewis acids and organometallic compounds are the most commonly used catalysts for the transesterification reactions.[12–14] Although these homogeneous catalysts are generally catalytically efficient, they are not cost-efficient because of their corrosive nature, low thermal stability, and critical issue in separation and recovery. Therefore, increasing attention has been paid to develop easily separable and reusable heterogeneous catalysts with high catalytic activities.[18–22] Over the past decade, supported metal oxide catalyst systems have been widely studied by virtue of their numerous applications and readiness for separation, recovery, and recycle.[18–21] Considerable efforts have been devoted to investigate the structural features of supported metal oxide catalysts and to find a correlation between physicochemical properties and catalytic performances. The supported metal oxides are commonly found to exhibit much better catalytic performances than the corresponding bulk metal oxides because of their cooperation with support. Moreover, it is easy to design or modify a specific supported metal oxide catalyst for a particular process. Generally, effective and convenient approaches for catalyst development are optimization of preparative variables such as loadings, calcination temperature, and support material. Particularly, the nature of the catalyst support plays an important role in catalytic behavior. It has been demonstrated that the support material can modify chemical properties and surface texture of the catalyst by itself or through interactions with the active phase, besides providing uniform structure, sufficient specific surface, and high thermal stability.[23,24] Therefore, an understanding and control of the interactions between active phases and support is essential in the development and optimization of supported metal oxide catalysts.

Recently, TiO_2-based catalysts have received great attention because of their remarkable catalytic activity for a wide variety of reactions such as photocatalytic reactions,[25–27] hydrodesulfurization (HDS) reactions,[28] selective catalytic reduction (SCR),[29] and transesterification.[30] Our previous work showed that TiO_2/SiO_2 catalysts, which were prepared by an impregnation method using toluene solution of tetrabutoxytitanium as precursors, are catalytically active in the transesterification of DMO with phenol.[21] It was suggested that the surface TiO_2 species and weak Lewis acid sites corporately contributed to the high activity and selectivity of TiO_2/SiO_2 catalysts in the transesterification of DMO with phenol.[31]

As a continuation of the previous work,[21,31] this study focuses on the preparation and optimization of highly dispersed supported TiO_2 catalysts made via a two-step wet impregnation method, which consists of an incipient impregnation of silica supports with an anhydrous ethanol solution of a titanium precursor and a subsequent hydrolysis treatment. Supported TiO_2/SiO_2 catalysts with different TiO_2 loadings and calcination temperatures were comparatively investigated. To gain a better understanding of surface properties of TiO_2/SiO_2 catalysts and their relationship with physicochemical and catalytic behaviors, a detailed characterization was performed by means of BET, SEM, ICP, XPS, XRD, Raman, FTIR of pyridine adsorption, and NH_3-TPD. In the second part of this article, the effects of various reaction parameters such as molar ratio of reactants, catalyst amount, reaction temperature, reaction time, and catalyst recycling on the catalytic performance were examined to

optimize DMO conversion and selectivity to the target products, MPO and DPO. A comparison of catalytic performances and acid properties of various solid catalysts was carried out. The results permit us to propose a mechanism for Lewis acid catalyzed transesterification of DMO with phenol. Additionally, for the first time, we present results of an investigation on the disproportionation reaction of MPO to DPO via a catalytic distillation process, which combines reactive distillation and heterogeneous catalysis.

Experimental

Catalyst preparation

Tetrabutoxytitanium ($Ti(OC_4H_9)_4$, TBT), DMO, anhydrous ethanol, and phenol were of laboratory reagent grade and purchased from local suppliers. Commercial silica (Jiangyan City Chemical Auxiliary Factory of China, particle size: 100–200 mesh) was used as a support material. Before impregnation, the silica supports were pretreated at 120°C for 2 h to remove physisorbed water.

Supported TiO_2 catalysts (with TiO_2 loadings in the range of 1–20 wt %) were prepared by a two-step wet impregnation method. First, the desired amount of TBT was dissolved in 50-mL anhydrous ethanol followed by addition of stoichiometric amounts of silica with vigorous stirring. Absence of water at this stage prevents the premature hydrolysis of the precursor. The obtained mixture was stirred and kept in flowing N_2 until adsorption equilibrium was established. Then deionized water was added drop by drop to obtain a molar ratio of TBT:H_2O = 1:4. Following the wet impregnation, products were allowed to age at room temperature for 24 h to facilitate hydrolysis of TBT. The resultant slurry was centrifuged and the solid fraction was heated in a vacuum oven at 120°C for 4 h. The dried material was subsequently calcined in an open-air furnace at 550°C for 5 h. To investigate the effect of calcination temperature, the samples with 12 wt % TiO_2 loading were calcined between 300 and 800°C.

Catalyst characterization

Specific surface areas and pore size distribution were determined on a constant volume adsorption apparatus (CHEMBET-3000) by N_2 physisorption at liquid nitrogen temperature. Prior to the measurements, all samples were degassed at 120°C for 5 h.

The morphology of the samples was examined using a scanning electron microscope (SEM, Philips XL 30 working at 10 kV). The samples were sputter coated with gold prior to scanning.

Elemental analyses of the catalysts (Ti, Si) were carried out with inductively coupled plasma-optic emission spectroscopy (ICP-OES) using a Varian VISTA-MPX spectrometer system. The sample was dissolved with requisite mixture of hydrogen fluoride and nitric acid in a platinum crucible. The crucible was covered and heated to 1000°C in a muffle furnace. After cooling at room temperature for 1 h, the clear solution was diluted in a HNO_3:HF:H_2O (1:1:1) mixture and was then ready for analysis.

X-ray photoelectron spectroscopy (XPS) was employed to determine the surface composition and the dispersion of active species. The measurements were carried out on a Perkin-Elmer PHI 1600 ESCA system with Mg Kα (1253.6 eV) radiation as the excitation source. The sample was placed onto a specimen holder via a double-sided adhesive tape. To eliminate charging effect, calibration of binding-energy was accomplished with respect to the internal standard of the C_{1s} peak (284.5 eV). Scanning of the spectra was done at room temperature under ultrahigh vacuum (UHV, $\sim 1.33 \times 10^{-8}$ Pa).

Crystalline phase was identified by X-ray diffraction (XRD) pattern recorded on a Rigaku C/max-2500 diffractometer using graphite filtered Cu Kα radiation (k = 0.15405 nm) at 40 kV and 100 mA. Scanning range was 10°–80° (2θ) with a step size of 0.05° with a count time of 1 s. The phases present in the samples were confirmed with the help of JCPDS files.

Raman spectra were obtained on a BRUKER RFS 100/S FT-Raman spectrometer using Nd: YAG laser at 1064 nm of 300 mW output as the emission source. The Raman spectra were recorded from 100 to 1400 cm^{-1} at room temperature.

IR spectroscopic measurements of adsorbed pyridine were carried out on a Bruker VECTOR22 FTIR spectrometer. The powdered catalysts were pressed into a 10 mg cm^{-2} self-supporting wafer. Prior to each experiment, the samples were evacuated (1 Pa) at 150°C for 3 h. Following this, the materials were exposed to 4×10^3 Pa of pyridine at 150°C for 1 h, and then flushed with flowing Ar for 30 min to remove the physisorbed pyridine. After adsorption, the samples were out-gassed and the spectra were recorded at room temperature. The scanning range was from 500 to 4000 cm^{-1} and the resolution was 4 cm^{-1}.

Acid site concentration and distribution of the catalysts were measured by temperature-programmed desorption of ammonia (NH_3-TPD), using a chemical adsorption spectrometer (Model 2910, Micromeritics Co.). The samples were placed in a quartz tubular reactor and pretreated at 500°C in flowing Ar for 1 h, and then cooled to 50°C. The pulses of NH_3 were supplied to the samples until saturation. Subsequently, a flow of Ar was passed through the reactor for 30 min to remove excessive physisorbed NH_3 from the samples. Desorption of NH_3 was monitored by ramping the temperature from 50 to 600°C at a rate of 10°C min^{-1}.

Transesterification of DMO with phenol

Transesterification of DMO with phenol was carried out in a 250-mL three-neck, round-bottomed flask, which is equipped with a thermocouple, an electromagnetically driven stirrer, a nitrogen inlet, and a reflux condenser. The reflux condenser was connected to a closed programmable circulator and was kept at 80°C by flowing recycled hot water in order to remove formed methanol from the reaction system. In a typical experiment, 0.1 mol of DMO, 0.3 mol of phenol, and 1.8 g of catalysts were fed to the reactor under nitrogen atmosphere. The resultant mixture was then heated to the reaction temperature (i.e., 180°C) at atmospheric pressure. After reaction, qualitative and quantitative analyses of reaction products and distillates were carried out on a SP3420 gas chromatograph equipped with a flame ionization detector (FID). An HP-5 capillary column (Hewlett-Packard, 15 m $\times$ 0.53 mm $\times$ 1.5 μm) was used to separate products for gas chromatographic analysis. HPLC grade acetone was used as

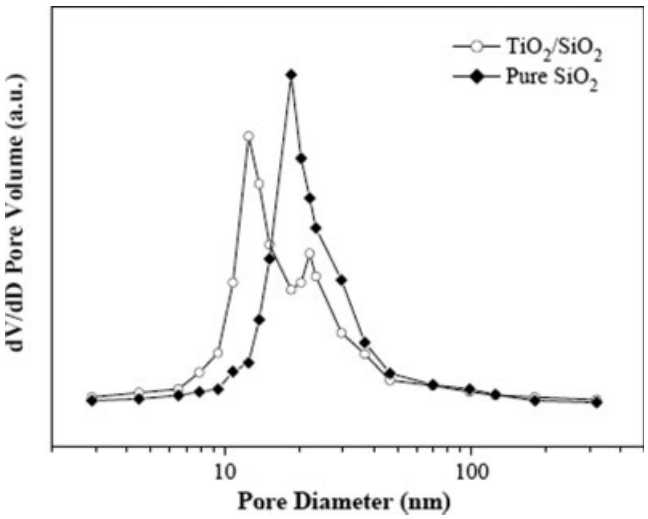

Figure 1. The pore size distribution curves of the TiO_2/SiO_2 sample and silica support.

a mobile phase, in which a small amount of ethyl benzoate was chosen as an internal standard reagent. DPO, MPO, and by-product anisole (AN) from the transesterification were quantified by comparing the peak areas with their corresponding standards.

Catalytic distillation

Catalytic distillation was employed to increase DPO production from the disproportionation. The experiments were conducted in a round-bottomed flask (500 mL), which is equipped with a rectification column, an oil-cooled reflux condenser, an electromagnetically driven stirrer, a thermometer, and a pressure gauge. The central part is the cylinder column with a 6.5 cm inner diameter and a packing height of 1 m. The reflux condenser was kept at 150°C by flowing recycled hot oil in order to remove methanol, phenol, and DMO from the reaction system. The reagents were the products obtained from the transesterification reaction and the catalyst was 12 wt % TiO_2/SiO_2. The desired pressure was achieved by means of a vacuum pump connected to the pressure gauge. The measured temperature was the equilibrium temperature corresponding to surrounding pressure. After 5 h, the reaction products were identified and quantified by GC analysis.

Results and Discussion

Characterization of the catalysts

Figure 1 shows the pore size distribution of TiO_2/SiO_2 catalyst (12 wt % TiO_2 loading) calcined at 550°C and silica support. It can be seen that the pore size range of the supported catalyst and silica are of the same dimension. The pore size distribution of TiO_2/SiO_2 is in the mesoporous region (8–40 nm) with an average pore size of 12.5 nm. As reported in our previous work,[21] the molecular sizes of DMO and phenol are $X = 0.6399$ nm, $Y = 0.5064$ nm and $X = 0.7122$ nm, $Y = 0.4915$ nm, $Z = 0.2532$ nm, respectively. For MPO and DPO, the molecular sizes are as follows: $X = 0.8432$ nm, $Y = 0.6327$ nm, $Z = 0.5609$ nm and $X = 0.9852$ nm, $Y = 0.5736$ nm, $Z = 0.4581$ nm, respectively. Thus, internal surfaces of the TiO_2/SiO_2 catalyst could be accessible to DMO and phenol molecules. Simultaneously, the produced MPO and DPO could return to the reaction system efficiently. Therefore, the active sites located in internal surface of the pore channels could be utilized equally to those located in external surface of the catalyst.

The supported oxides usually possess different surface and textual properties from the bulk oxides. The BET surface area of the silica support with the same heat treatment as TiO_2/SiO_2 catalyst was found to be 231 $m^2\ g^{-1}$. As shown in Table 1, The BET surface area of TiO_2/SiO_2 increased initially with increasing TiO_2 loading up to 12 wt %, and then decreased sharply at higher loadings. Figure 2 shows the typical SEM photographs of the silica support and supported catalyst (12 wt % TiO_2 loading). The particle size of TiO_2/SiO_2 (Figure 2b) is smaller than that of the silica (Figure 2a). However, there is no obvious difference in the morphological features between silica and the supported catalyst, indicating the good quality of the supported catalysts prepared by wet impregnation method.

The prepared TiO_2/SiO_2 catalysts containing different TiO_2 contents were characterized by ICP and XPS. The elemental compositions of TiO_2/SiO_2 catalysts and binding energies (BE) of Ti $2p_{3/2}$ are summarized in Table 1. It is well known that the XPS intensity ratio of active compound to support could be used to predict the dispersion capacity of supported metal oxide catalysts.[32,33] The XPS intensity ratio of Ti 2p to Si 2p ($I_{Ti\ 2p}/I_{Si\ 2p}$) were plotted vs. actual Ti/Si atomic content ratio (X_{Ti}/X_{Si}) measured by ICP (see Figure 3). It can be seen that $I_{Ti\ 2p}/I_{Si\ 2p}$ ratio increases with an increase in TiO_2 loadings. However, this increase is not proportional to the X_{Ti}/X_{Si} ratio. Two lines can be linearly regressed from the experimental data and give a point of intersection at 0.16 Ti/Si g g^{-1}. According to a monolayer model proposed by Kerkhof and Moulijn,[32] a linear relation can be established between XPS intensity ratio and bulk atomic ratio of the active phase and the support for monolayer catalysts as well as for catalysts with crystallites of constant sizes. Thus, the intersection shown in Figure 3 represents the change of dispersion state of surface titanium oxide from monolayer to crystalline. The monolayer capacity

Table 1. Physicochemical Properties of the TiO_2/SiO_2 Catalysts with Different TiO_2 Loadings

TiO_2 Loadings (wt %)	S_{BET}* ($m^2\ g^{-1}$)	X_{Ti}/X_{Si}† (g g^{-1})	TiO_2 amount‡/ atoms nm^{-2} (SiO_2)	$I_{Ti\ 2p}/I_{Si\ 2p}$	BE Ti $2p_{3/2}$ (eV)
1	228	0.01	0.30	0.01	460.8
5	231	0.05	1.30	0.04	459.4
10	234	0.10	2.64	0.09	459.3
12	239	0.13	3.35	0.11	459.1
14	225	0.16	4.12	0.14	459.1
16	209	0.19	4.80	0.14	458.8
20	168	0.26	6.55	0.16	458.7
100	31	—	—	—	458.5

*The surface areas of the catalysts calcined at 550°C.
†Actual grams of titanium by gram of silicon obtained by Inductively Coupled Plasma (ICP).
‡Atoms of titanium by surface area; I_{Ti2p}/I_{Si2p}: XPS intensity ratio; BE: binding energies of $Ti_{2p3/2}$ peak.

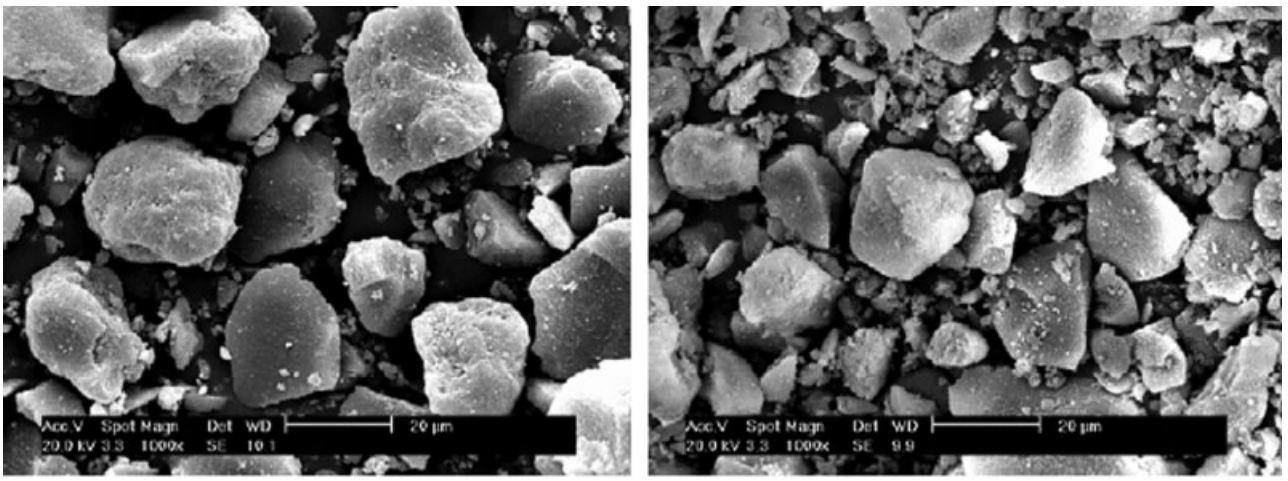

Figure 2. SEM photographs of surfaces of (a) silica and (b) 12 wt % TiO_2/SiO_2 catalyst.

of TiO_2 on silica is thus estimated to be about 4.01 TiO_2 molecules nm^{-2} (SiO_2), which is in agreement with the experimental data reported by Gao et al.[34]

Another issue we need to address here is that BE values of Ti $2p_{3/2}$ decreased with an increase of TiO_2 loadings (Table 1). Many researchers have reported on the bonding interactions between the dispersed titanium oxide species and silica.[34–39] These investigations show that the formation of chemical bonds such as Ti—O—Si can significantly influence the electronic structure of surface titanium species. The presence of more electronegative element, Si, in the neighbor of Ti could cause a shift of Ti $2p_{3/2}$ BE toward higher values.[35–37] Thus, the relatively high Ti $2p_{3/2}$ BE at low loadings compared with pure TiO_2 (458.5 eV) could be due to the high dispersion of TiO_2 and to the interaction bonds between titanium species with silica (Ti—O—Si). As TiO_2 loading was increased above the monolayer capacity, the BE values of the samples shifted toward that of the pure TiO_2 (i.e., 458.8 eV at 16 wt %), indicating that the formation of bulk TiO_2 were predominate at higher TiO_2 loadings.[40]

These XPS results evidence the presence of interaction between surface titanium oxide and silica through formation of the Ti—O—Si bonds. The bonding interactions between the active phase and the support are initially developed during the impregnation (i.e., the titanic precursor interacted with the hydroxyl groups on silica). Subsequent hydrolysis of the precursor and oxidative treatment at high temperatures lead to the dispersion of active species on support. The titanium oxide species strongly bonded with silica surface can be well dispersed on the catalyst, whereas a weak interaction with the support may lead to poor dispersion and formation of bulk TiO_2 out of surface coverage. As such, dispersion and chemical state of surface titanium oxide species can be intimately correlated to their bonding interactions with the support surface.

The phase compositions of the samples were further confirmed by XRD measurements. The XRD patterns of TiO_2/SiO_2 with various TiO_2 loadings and a reference pure anatase TiO_2 are presented in Figure 4. The diffractograms suggest the absence of characteristic peaks of TiO_2 in the samples with TiO_2 loadings of 12 wt % and below. However, the anatase peaks (JCPDS 12-1272) can be detected for the samples at TiO_2 loadings more than 12 wt %, and the peak intensities increased with TiO_2 loadings. On the other hand, no detectable diffraction peaks of TiO_2 at lower loadings may not necessarily due to high dispersion of TiO_2 phase, but to the presence of nanosized TiO_2 crystallites that do not show X-ray diffraction. Additional XRD characterization was performed on a mechanical mixture of TiO_2 nanoparticles (with diameters of 10–30 nm) and silica with 1 wt % TiO_2 content. The results showed that nanosized TiO_2 particles can be detected by XRD (data not shown). These observations indicate that TiO_2 species exist in highly dispersed state on the silica surface at loadings below 14 wt %. Further increasing loading level leads to the formation of TiO_2 crystallites besides the surface-dispersed titanium oxide species. The bulk TiO_2 crystallites could physically blocked the pore mouths of the catalyst, leading to the decrease in surface area.

Raman spectra of TiO_2/SiO_2 samples are shown in Figure 5. The main features in the Raman spectra changed at load-

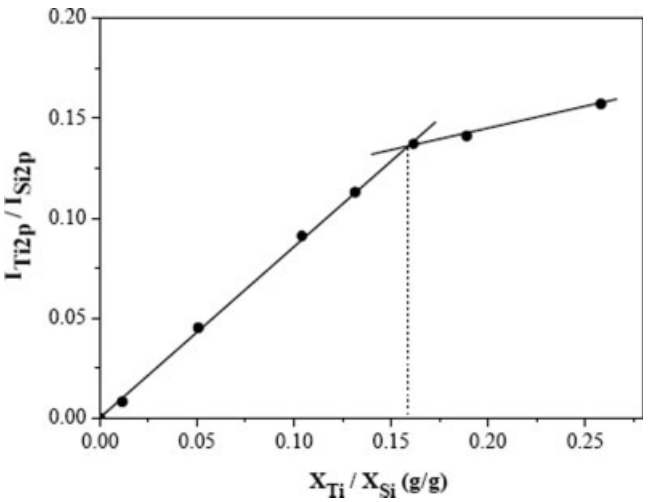

Figure 3. Relationship between $I_{Ti\ 2p}/I_{Si\ 2p}$ and X_{Ti}/X_{Si}.

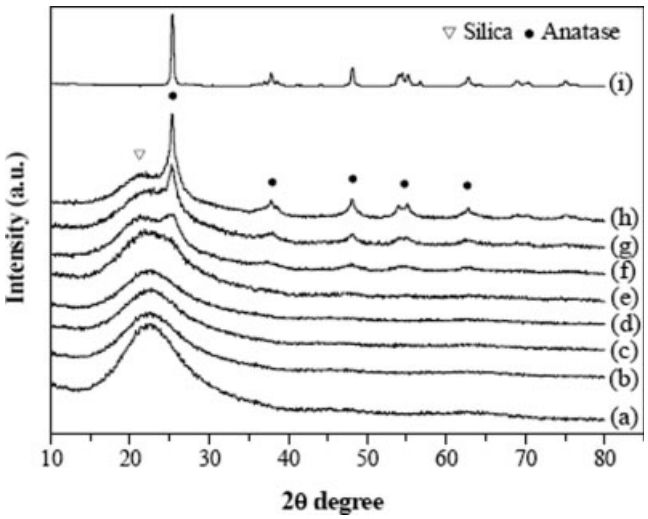

Figure 4. XRD patterns of TiO_2/SiO_2 catalysts with different TiO_2 loadings: (a) support; (b) 1%; (c) 5%; (d) 10%; (e) 12%; (f) 14%; (g) 16%; (h) 20%; and (i) nanoanatase TiO_2.

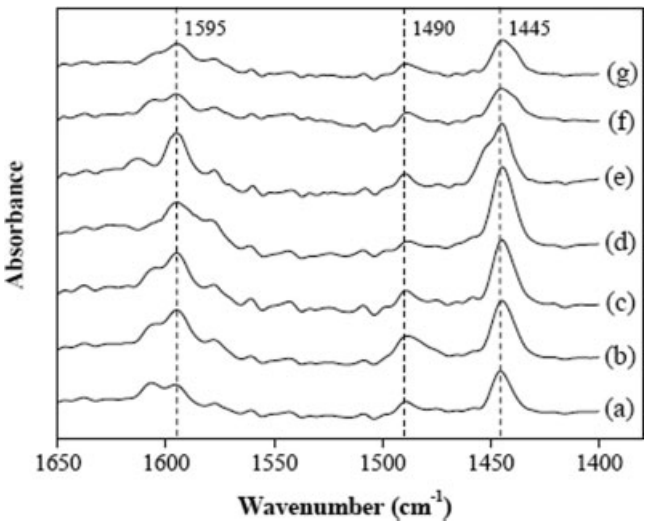

Figure 6. FTIR spectra of pyridine absorbed on TiO_2/SiO_2 catalysts with different TiO_2 loadings: (a) 1%; (b) 5%; (c) 10%; (d) 12%; (e) 14%; (f) 16%; and (g) 20%.

ings between 12 and 14 wt %. For TiO_2/SiO_2 with 14 wt % and higher loadings, characteristic 146 cm^{-1} band corresponding to the TiO_2 anatase phase appeared and its intensity increased with the increase of TiO_2 loadings. This is well agreed with our XRD results, indicating that TiO_2 species were present on the silica surface in highly dispersed state at lower TiO_2 loadings and bulk crystalline TiO_2 formed above the monolayer capacity of surface titanium oxide. Combining these results obtained from various characterization techniques, not only is it successful to detect the effect of TiO_2 loading on surface properties of TiO_2/SiO_2 catalysts, but it is feasible to identify the dispersion capacity of TiO_2 on SiO_2.

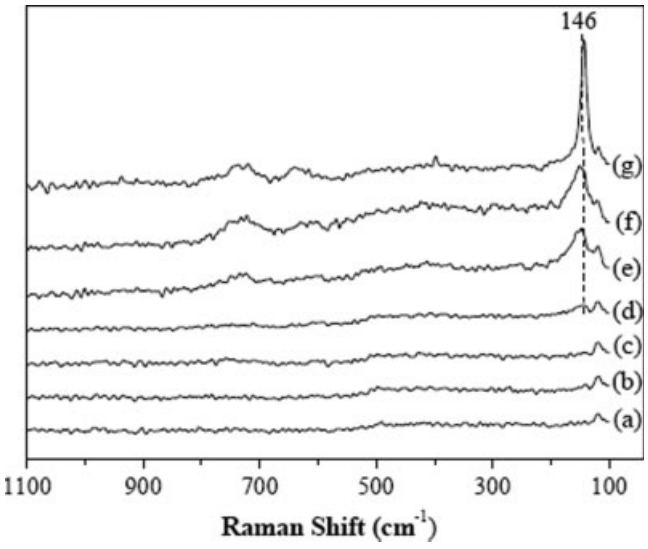

Figure 5. Raman spectra of TiO_2/SiO_2 catalysts with different TiO_2 loadings: (a) 1%; (b) 5%; (c) 10%; (d) 12%; (e) 14%; (f) 16%; and (g) 20%.

It has been known that many base molecules, such as pyridine and ammonia, can react with surface acid sites and therefore are often used to qualitatively and quantitatively determine different types of acid site.[41–43] In this work, characterization of Brönsted (B) and Lewis (L) acid sites and their relative amount in the samples were carried out based on the FTIR analysis of adsorbed pyridine. The normalized IR spectra (band intensities normalized against sample weight) of adsorbed pyridine on TiO_2/SiO_2 catalysts are shown in Figure 6. Absorption bands near 1445 and 1595 cm^{-1} representing pyridinium ions and pyridine molecules coordinated with L-acid sites can be observed in all spectra. The peak intensity is considerably sensitive to the increase of TiO_2 loading. Another feature appearing at 1490 cm^{-1} can be assigned to the overlapping of B- and L-acid sites. However, the band around 1545 cm^{-1} attributed to B-acid sites is absent for all the samples. This indicates that there mainly exist L-acid sites on the surface of TiO_2/SiO_2 catalyst, while B-acid sites are almost negligible.

The amount of L-acid sites on TiO_2/SiO_2 catalysts was quantitatively determined in terms of relative band area. As shown in Table 2, the amount of L-acid sites on TiO_2/SiO_2 catalysts increased with increasing TiO_2 loadings from 1 to 12 wt %, then decreased slightly with the further deposition

Table 2. Effect of TiO_2 Loading on the Comparative Acid Amounts Associated with Lewis Acid Sites

TiO_2 Loading (wt %)	Amounts of Comparative Acid (mmol mg^{-1})
1	325.2
5	479.6
10	582.3
12	596.7
14	592.4
16	588.3
20	581.5

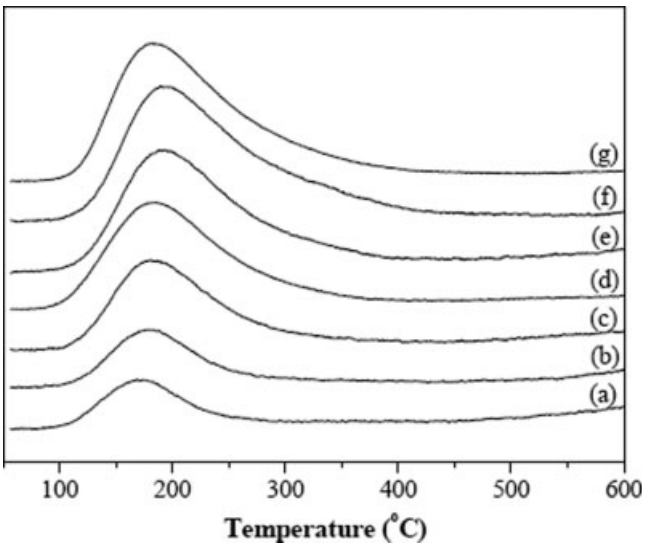

Figure 7. NH_3-TPD profile of TiO_2/SiO_2 catalysts with different TiO_2 loadings: (a) 1%; (b) 5%; (c) 10%; (d) 12%; (e) 14%; (f) 16%; and (g) 20%.

of TiO_2. At TiO_2 loading less than the monolayer capacity, increasing TiO_2 loading means the increase of highly dispersed titanium oxide species and the resultant increase of the amount of acid sites on TiO_2/SiO_2 catalysts. At higher TiO_2 loadings, even though bulk TiO_2 crystallites could also provide a few acid sites, the number of acid sites from crystalline TiO_2 was much less than that from dispersed TiO_2, which led to a decrease of acid sites amount. On the basis of these results, we speculate that the monolayer-dispersed TiO_2 could contribute more L-acid sites than bulk TiO_2 crystallites.

NH_3-TPD was performed to survey the acid strength of the TiO_2/SiO_2 catalysts. In NH_3-TPD curves, the peaks are generally distributed into three regions according to ammonia desorption temperatures: low temperature (LT) region with peaks below 200°C, medium temperature (MT) region at 200–450°C, and high temperature (HT) region with peaks above 450°C. The peaks in LT, MT, and HT regions can be attributed to the desorption of NH_3 from weak, medium, and strong acid sites (Brönsted and/or Lewis), respectively.[42,43] From the results shown in Figure 7, the band corresponding to weak acid sites is observed for all the samples. Furthermore, the peak shifted toward higher temperatures with increasing TiO_2 loading and the maximum temperature offset is about 15°C. This suggests that TiO_2 loading has little effect on the strength of surface acid sites. Combination of FTIR studies of pyridine adsorption with NH_3-TPD results leads to the conclusion that there are only weak Lewis acid sites on the surface of TiO_2/SiO_2 catalysts.

Transesterification of DMO with phenol

Effect of TiO_2 Loading. The catalytic performances of TiO_2/SiO_2 catalysts as a function of TiO_2 loadings are presented in Table 3. The two major products are MPO produced via transesterification of DMO with phenol and DPO produced by disproportionation of MPO. DMO conversion increased on increasing TiO_2 loading up to 12 wt % and decreased at higher TiO_2 loadings. The similar behavior can be observed in the selectivity and yield of DPO, which attained maximum values of 25.3% and 16.8%, at 12 wt % TiO_2 loading. Comparatively, selectivity toward the intermediate product MPO reached a minimum at 12 wt % TiO_2 loading, indicating that much more MPO was converted into DPO over 12 wt % TiO_2/SiO_2 catalyst. The total selectivity to MPO and DPO remained more than 98.8% for all the catalysts, and GC analysis indicated that the major by-product was AN. Our earlier report has shown that the formation of AN and its isomers is due to the methylation of phenol and decarboxylation of methyl phenyl oxalate.[13]

The change of catalytic activity with TiO_2 loading could be explained on the basis of the surface properties of the TiO_2/SiO_2 catalysts. At TiO_2 loadings less than monolayer capacity, increasing TiO_2 loading generates more active catalytic sites to promote the transesterification. However, the catalytic activity is decreased apparently as bulk crystalline phase of TiO_2 appears in the high loading samples. The maximum activity is obtained at TiO_2 loading around the monolayer capacity, which is an example of so-called threshold effect. It can be speculated that compared with crystalline TiO_2, the monolayer-dispersed TiO_2 are more beneficial to the transesterification of DMO with phenol. On the other hand, we notice that there is a correlation between the surface acidity and catalytic performance: more Lewis acid sites yield higher catalytic activities (Tables 2 and 3). The above results demonstrate that the surface dispersed TiO_2 and amount of L-acid sites are two most important activity-determining factors for the transesterification of DMO with phenol. The formation of TiO_2 crystallites with consequent decrease in surface area and decrease in amount of acid sites at higher TiO_2 loading samples would be primarily responsible for the decrease of catalytic activity.

Effect of Calcination Temperature. The effect of calcination temperature on the surface properties and catalytic behavior of TiO_2/SiO_2 was studied. The XRD patterns of TiO_2/SiO_2 catalysts, where TiO_2 loading is 12 wt %, calcined at various temperatures are given in Figure 8. As can be seen, no TiO_2 diffraction peaks were observed at calcination temperatures below 550°C. The anatase peaks appeared at 600°C and after that the main peaks became more intense with the increase in calcination temperature. It can be explained that increasing calcination temperature improves

Table 3. Catalytic Activities of TiO_2/SiO_2 Catalysts with Different TiO_2 Loadings

TiO_2 Loadings (wt %)	Conversion* (%)	Selectivity (%)			Yield (%)	
		AN	MPO	DPO	MPO	DPO
1	42.9	0.6	80.8	18.3	34.3	7.9
5	51.5	0.6	76.7	22.7	39.5	11.7
10	62.3	0.7	74.2	25.0	46.2	15.6
12	66.3	0.6	73.9	25.3	49.0	16.8
14	65.9	0.7	74.1	25.1	48.8	16.5
16	62.4	0.8	75.2	23.4	46.9	14.6
18	56.8	0.9	76.4	22.5	43.4	12.9
20	50.8	1.0	77.4	21.4	39.3	10.9

Reaction conditions: 0.1 mol DMO, 0.3 mol phenol, 1.8 g catalyst (calcined at 550 °C), conducted at 180 °C for 2 h.
*Based on charged DMO.

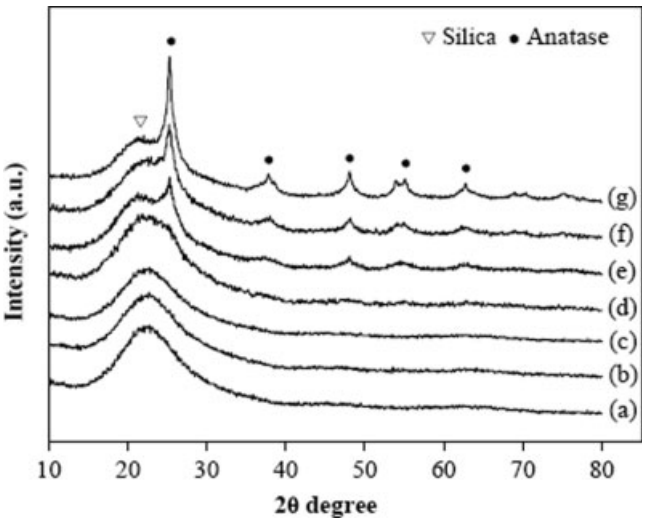

Figure 8. XRD spectra of 12 wt % TiO_2/SiO_2 catalysts under different calcination temperatures: (a) 300°C; (b) 400°C; (c) 500°C; (d) 550°C; (e) 600°C; (f) 700°C; and (g) 800°C.

the crystallinity and enhances the crystallite size of particles. Moreover, it is noted that distinct TiO_2 diffraction peaks appeared for the catalysts with 14 wt % TiO_2 loading calcined at 550°C (Figure 4) and 12 wt % loading calcined at 600°C (Figure 8). This further improve that TiO_2 species remain in a highly dispersed state on silica surface at 12 wt % TiO_2 loading and calcination temperature of 550°C. Figure 9 shows the surface area and average pore size of TiO_2/SiO_2 catalysts calcined at various temperatures. With the increase of calcination temperature from 300 to 800°C, the surface area was significantly reduced while the average pore size of samples increased from 3.4 to 32.2 nm. Such a decrease in surface area and the corresponding growth of pores could be attributed to the conglomeration of TiO_2 crystallites as well as the surface sintering as a result of calcination.

Table 4 shows the catalytic performances of the TiO_2/SiO_2 catalysts under different calcination temperatures. As can be

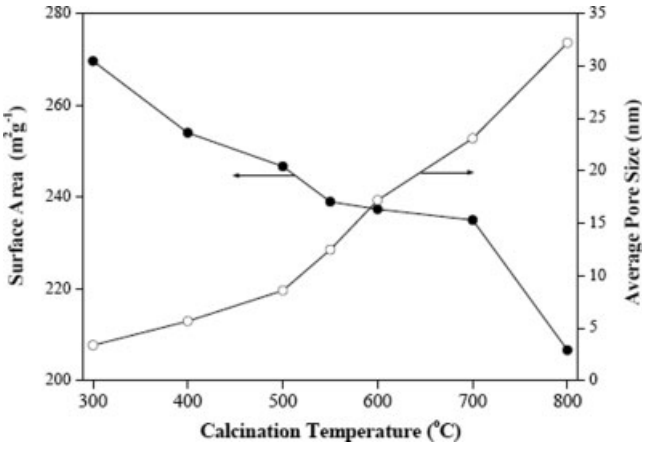

Figure 9. Surface area and average pore size of 12 wt % TiO_2/SiO_2 catalysts with different calcination temperature.

Table 4. Effect of Calcination Temperature on Catalytic Properties of TiO_2/SiO_2

Calcination Temperature (°C)	Conversion* (%)	Selectivity (%)			Yield (%)	
		AN	MPO	DPO	MPO	DPO
300	48.8	2.1	78.3	19.1	38.2	9.3
400	49.2	1.0	79.1	19.7	38.9	9.7
500	58.1	0.7	74.2	25.0	43.1	14.5
550	66.3	0.6	73.9	25.3	49.0	16.8
600	65.4	1.1	74.6	24.0	48.8	15.7
700	62.1	1.2	76.7	21.6	47.6	13.4
800	52.6	1.5	81.7	16.3	43.0	8.6

Reaction conditions: 0.1 mol DMO, 0.3 mol phenol, 1.8 g catalyst (12 wt% TiO_2 loading), conducted at 180 °C for 2 h.
*Based on charged DMO.

seen, the best activity is obtained for the catalyst calcined at 550°C, which is obviously due to the well-dispersed TiO_2 species and mesoporous structure on the silica surface. Considering DMO conversion and DPO selectivity, the catalyst with 12 wt % TiO_2 loading and calcination temperature of 550°C offered the best catalytic activity and was thus chosen as a model catalyst in the following sections to optimize reaction parameters.

Effect of Molar Ratio of Phenol to DMO. The reaction was carried out varying molar ratio of phenol to DMO from 1:1 to 5:1 by using the most active TiO_2/SiO_2 catalyst (12 wt % TiO_2 loading calcined at 550°C). Because the transesterification of DMO with phenol is an equilibrium limited reaction as shown by reaction 4, an excess amount of phenol is required to shift the equilibrium toward product formation. As shown in Table 5, the equilibrium conversion of DMO increased sharply from 1:1 to 3:1 (phenol/DMO molar ratio). However, further increase in the molar ratio above 3:1 had no appreciable effect on the activity. Thus, a large amount of excess phenol is not an essential condition to maximize the reaction productivity.

Effect of Catalyst Amount. Variation of amount of TiO_2/SiO_2 catalyst was also investigated for the transesterification. As shown in Table 6, very little DPO is formed in the absence of catalyst, suggesting the necessity of catalyst for the transesterification. DMO conversion increased rapidly until the catalyst amount reached 1.8 g, and then the conversion arrived at a plateau value with further increasing the catalyst amount. The selectivity to DPO kept increasing with the increase in catalyst amount from 0.3 to 1.8 g, but thereafter did not show a meaningful change.

Table 5. Effect of Molar Ratio of Phenol to DMO on Catalytic Properties of TiO_2/SiO_2

n(phenol): *n*(DMO)	Conversion* (%)	Selectivity (%)			Yield (%)	
		AN	MPO	DPO	MPO	DPO
1:1	48.7	1.5	80.2	17.7	39.1	8.6
1:2	59.9	1.2	76.5	21.9	45.8	13.1
1:3	66.3	0.6	73.9	25.3	49.0	16.8
1:4	67.3	0.8	73.0	25.9	49.1	17.4
1:5	68.1	0.7	72.5	25.7	49.4	17.5

Reaction conditions: 0.1 mol DMO, 1.8 g catalyst (calcined at 550 °C with 12 wt% TiO_2 loading), conducted at 180 °C for 2 h.
*Based on charged DMO.

Table 6. Effect of Catalyst Amount on Catalytic Properties of TiO_2/SiO_2

Amount of Catalyst (g)	Conversion* (%)	Selectivity (%)			Yield (%)	
		AN	MPO	DPO	MPO	DPO
0.0	1.43	5.2	84.6	0.0	1.21	0
0.3	48.3	0.6	78.3	18.9	37.8	9.1
0.6	55.5	0.5	78.2	20.1	43.4	11.2
1.2	60.9	0.6	76.7	22.5	46.7	13.7
1.8	66.3	0.6	73.9	25.3	49.0	16.8
2.4	66.9	0.7	73.8	25.2	49.4	16.9
3.0	67.3	0.9	73.6	25.0	49.5	16.8

Reaction conditions: 0.1 mol DMO, 0.3 mol phenol, catalyst (calcined at 550 °C with 12 wt% TiO_2 loading), conducted at 180 °C for 2 h.
*Based on charged DMO.

Effect of Reaction Temperature. From thermodynamic point of view, both the formation of MPO (reaction 4) and the production of DPO via the disproportionation of MPO (reaction 5) are endothermic processes,[19] which are favored at high temperatures. As shown in Table 7, there was a significant change in the catalytic properties of TiO_2/SiO_2 catalyst as reaction temperature increased from 150 to 180°C. At the temperatures below 180°C, a great amount of AN and other by-products, such as methyl phenol and benzyl alcohol, were found. Two possible routes of the by-products formation must be considered: methylation of phenol (reaction 6) and decarboxylation of MPO (reaction 7).[13] Because of the restriction of the boiling point of reactants, the highest reaction temperature at atmosphere pressure is around 180°C. Thus, 180°C is chosen as the operation temperature at ambient condition.

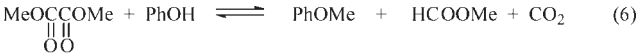

$$\mathrm{MeOCCOMe} + \mathrm{PhOH} \rightleftharpoons \mathrm{PhOMe} + \mathrm{HCOOMe} + \mathrm{CO_2} \quad (6)$$

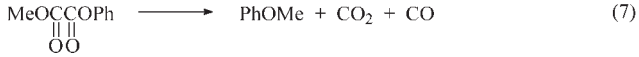

$$\mathrm{MeOCCOPh} \longrightarrow \mathrm{PhOMe} + \mathrm{CO_2} + \mathrm{CO} \quad (7)$$

Effect of Reaction Time. To investigate the effect of reaction time on the transesterification, samples of the reacting mixture were collected at certain intervals and analyzed. As shown in Figure 10, DMO conversion increased sharply from 0.5 to 2 h, and then gradually leveled off with the reaction time up to 10 h. With increasing reaction time, selectivity to MPO decreased continually while selectivity to DPO was distinctly improved, indicating that much more DPO was formed via disproportionation of MPO with the time of reaction. In addition, selectivity of by-products increased with the reaction time, reaching about 10.6% at 10 h. This is probably due to the side reactions described in reactions 6 and 7.

Table 7. Effect of Reaction Temperature on Catalytic Properties of TiO_2/SiO_2

Reaction Temperature (°C)	Conversion* (%)	Selectivity (%)			Yield (%)	
		AN	MPO	DPO	MPO	DPO
150	26.3	11.3	66.5	16.0	17.5	4.2
160	43.2	10.6	66.7	17.1	28.8	7.4
170	59.8	9.4	67.4	17.9	40.3	10.7
180	66.3	0.6	73.9	25.3	49.0	16.8

Reaction conditions: 0.1 mol DMO, 0.3 mol phenol, 1.8 g catalyst (calcined at 550 °C with 12 wt% TiO_2 loading), conducted for 2 h.
*Based on charged DMO.

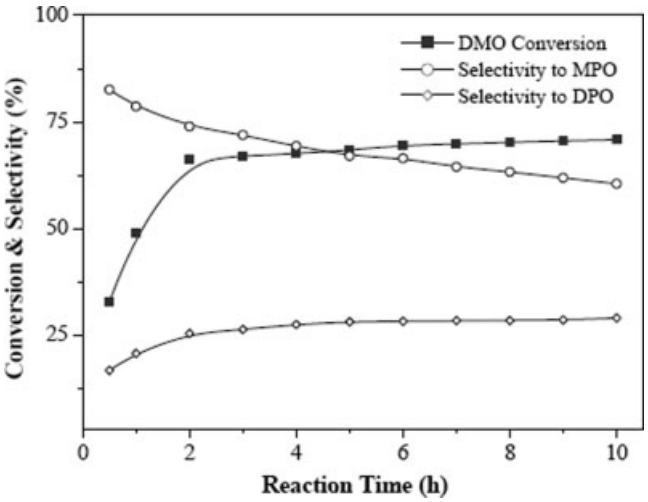

Figure 10. Effect of reaction time on catalytic properties of TiO_2/SiO_2; reaction conditions: 0.1 mol DMO, 0.3 mol phenol, 1.8 g catalyst (calcined at 550°C with 12 wt % TiO_2 loading), conducted at 180°C.

Reaction Kinetic Studies. To obtain the kinetic information of the transesterification of DMO with phenol, the reaction kinetics was investigated in terms of reaction time and temperature under otherwise identical conditions. Plots of $-\ln$ (1 − DMO conversion) vs. the reaction time at different temperatures ranging from 150 to 180°C are given in Figure 11a. The plots are nearly linear in all the cases, indicating first-order behavior of the transesterification. The slops of these plots gave the reaction rate constants (k) at each temperature. The rate constant was apparently increased by raising the temperature. Figure 11b shows the Arrhenius plot of $\ln k$ vs. $1/T$. The plot was linear and the activation energy for the TiO_2/SiO_2 catalyst was derived from the slope to be 36.76 kJ mol^{-1}.

Catalyst Recycling. The recyclability of heterogeneous catalysts is a great concern in industrial catalytic processes, meaning that a good catalyst should remain its activity and selectivity at high levels over times of reuse. After each recycle, the catalyst was separated from the reaction mixture by filtration and washed by anhydrous ethanol to remove accumulated organic compounds from the catalyst. Further, the catalyst was dried overnight followed by calcination at 550°C for 5 h, and then reused with fresh reaction mixture. Considering the catalyst loss during each recycle, catalysts reused were collected from two identical runs to obtain exactly same amount of catalyst used in a previous experimental test. Table 8 illustrates the activities of recycled catalysts under otherwise identical conditions. It was found that DMO conversion slightly dropped from 66.3% to 63.4% after the fourth recycle and further to 59.2% after the sixth recycle. The total selectivity of MPO and DPO slightly decreased and still remained above 97% after six recycles.

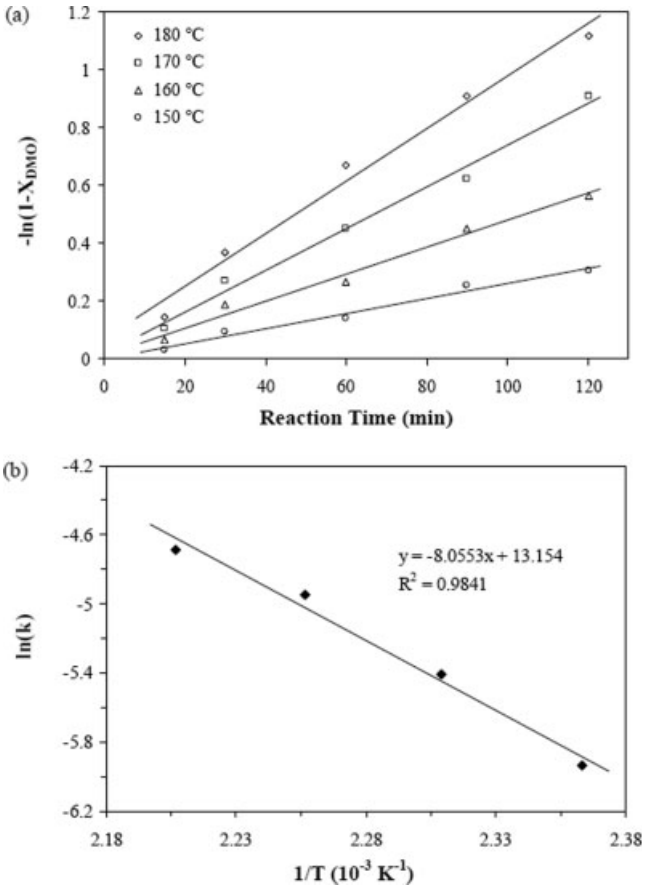

Figure 11. (a) Kinetic plots for the transesterification over TiO_2/SiO_2 at different temperatures; (b) Arrhenius plot.

Clearly, the major loss of catalytic activity was observed from the forth to the sixth recycle. According to ICP and XPS analyses of the recovered catalysts, although there was no significant change in Ti/Si ratio up to six recycles (indicating strong Ti—O—Si bonding between titanium species and silica), carbon composition was increased with increasing the number of recycles. The formation of carbonaceous deposits over the catalyst surface is derived from the decomposition of organic compounds absorbed on the catalyst. Additionally, BET analysis show that recycling exerts a noticeable influence in textural properties of the catalysts such as specific surface area and pore size distribution. After the sixth recycle, the specific surface area decreased from 239 $m^2\ g^{-1}$ of the fresh catalyst to 217 $m^2\ g^{-1}$ and the average pore size decreased from 12.5 to 10.8 nm, suggesting pores are partially plugged during the recycling. These changes may be due to carbon deposition on the catalyst surface, another possible reason could be that the texture and structure of the catalysts were partly destroyed by successive and invasive regeneration procedure.

Table 8. Recyclability of TiO_2/SiO_2 Catalysts for the Transesterification

Number of Recycling	Conversion* (%)	Selectivity (%)			Yield (%)	
		AN	MPO	DPO	MPO	DPO
0	66.3	0.6	73.9	25.3	49.0	16.8
1	65.6	0.8	74.0	24.9	48.5	16.3
2	64.8	1.0	73.8	24.7	47.8	16.0
4	63.4	1.1	73.5	24.4	46.6	15.5
6	59.2	1.8	73.1	23.9	43.3	14.1

Reaction conditions: 0.1 mol DMO, 0.3 mol phenol, 1.8 g retrieved TiO_2/SiO_2 catalyst, conducted at 180°C for 2 h.
*Based on charged DMO.

Comparison of the Catalytic Performances with Different Catalysts. For comparison purposes, various solid catalysts were evaluated in the transesterification reaction under the selected reaction conditions. As shown in Figure 12, $AlCl_3$ showed relatively high DMO conversion (79.8%) but very low selectivity to the target products. Silica is well known as a support material for its stable properties and large surface area. Although SiO_2 showed feeble activity for this reaction, it is the preferred carrier because it afforded excellent selectivity to MPO as high as 100%. Both MoO_3 and Al_2O_3 exhibited high levels of DMO conversion, i.e., DMO conversion was 67.9% over Al_2O_3. However, MoO_3 and Al_2O_3 were so poor in selectivity to target products that the total selectivities were 55.6% and 38.8%, respectively. SnO_2 gave very high selectivity to MPO and DPO (57.1% and 35.7%) but only 2.8% DMO conversion. TiO_2 is an efficient catalyst for the transesterification, giving ~35% DMO conversion as well as 99% total selectivity to MPO and DPO. From these results, it seems that the selectivity of the catalyst is strongly dependent on their acidic nature. Strong acid catalysts, such as $AlCl_3$ and Al_2O_3, tend to favor the undesired formation of AN or other by-products.

To verify the potential of TiO_2-based catalyst systems, different supported TiO_2 catalysts with 12 wt % TiO_2 loading were prepared and employed to catalyze the transesterification (Figure 12G–L). All of these supported TiO_2 catalysts

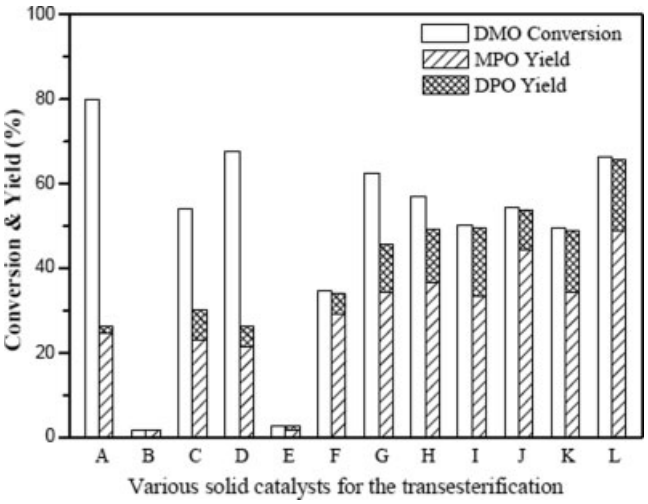

Figure 12. Comparison of catalytic activities of various solids catalysts for the transesterification: A, $AlCl_3$; B, SiO_2; C, MoO_3; D, Al_2O_3; E, SnO_2; F, TiO_2; G, TiO_2/MgO; H, TiO_2/Al_2O_3; I, TiO_2/SiO_2-Al_2O_3; J, TiO_2/C; K, TiO_2/TS; and L, TiO_2/SiO_2.

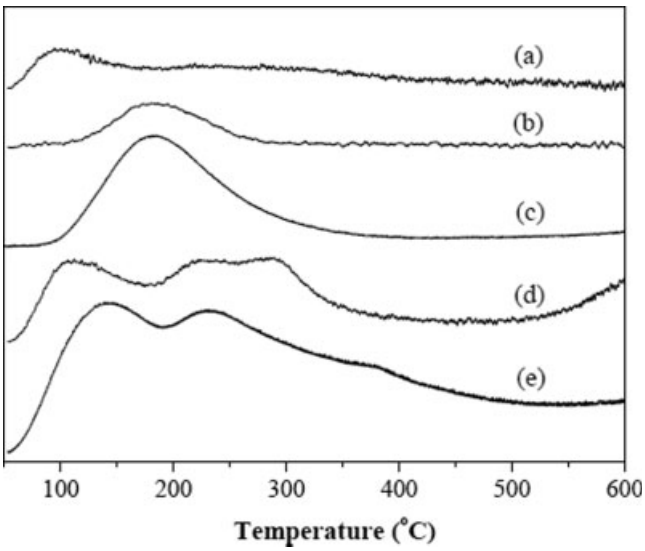

Figure 13. NH_3-TPD profile of the different oxide catalysts: (a) SiO_2; (b) TiO_2; (c) TiO_2/SiO_2; (d) TiO_2/MgO; and (e) TiO_2/Al_2O_3.

seem to be superior to pure TiO_2 owing to the increased specific area and better dispersion of TiO_2 active centers. However, the selectivity to AN was comparatively high over TiO_2/Al_2O_3 and TiO_2/MgO, indicating that the properties of support materials (i.e., acidity) may play a significant role in the selective formation of the target products and by-products. Among these supported catalysts, TiO_2/SiO_2 exhibited the best performance on both DMO conversion and total selectivity to the target products.

To better understand the relationship between surface acidity and catalytic behavior, NH_3-TPD measurements were carried out on silica, titania, and supported TiO_2 catalysts. As shown in Figure 13, the ammonia desorption peak of SiO_2, TiO_2, and TiO_2/SiO_2 just appears in the low temperature region, confirming that there exist only weak acid sites on the solid surface. For TiO_2/MgO and TiO_2/Al_2O_3, the NH_3-TPD patterns show broad desorption signals corresponding to acid sites with weak strength (LT region) and medium strength (MT region), suggesting coexistence of weak and medium acid sites. Combining with the results of NH_3-TPD and product distribution, it could be concluded that acidic nature of the catalyst is a key factor in determining the selectivity to desired products. TiO_2 and TiO_2/SiO_2, in which only weak acid sites exist, show significantly high total selectivity to target products. In the case of TiO_2/MgO and TiO_2/Al_2O_3, high selectivity to by-products may be attributed to the presence of intermediate acid sites on the catalysts. Thus, we speculate that the weak acid sites are responsible for the formation of MPO and DPO, whereas the intermediate acid sites are in favor of the formation of by-products, i.e., AN.

According to the above results and discussion, a plausible reaction mechanism for the transesterification of DMO and phenol over Lewis acid sites was proposed, as described in Scheme 1. The active species, TiO_2, act as Lewis acid (LA) in the cleavage of acyloxy bond. The coordination of the carbonyl group in DMO with Lewis acid sites transfers electron density in DMO to metal ion. This effect results in the carbon atom in carbonyl easily attacked by the weak nucleophilic reagent, phenol, and consequently produces a four-center intermediate between DMO and phenol. In the last step, the four-center intermediate lost methanol molecule, resulting in the formation of MPO. Thus, the catalytic circle of Lewis acid sites and the ester exchange are completed. From Scheme 1, it should be noted that the approach of phenol to the carbonyl carbon of DMO would be affected by steric hindrance. Especially, further attack of ortho carbonyl group could be retarded by the greater steric effect as the reactant molecules become more bulky. This gives the reason responsible for relatively low selectivity to DPO even though the molar ratio of phenol to DMO, catalyst amount, and reaction time have been increased to high values.

Applying catalytic distillation to DPO synthesis

In addition to the above discussed steric hindrance, thermodynamic equilibrium restriction also plays an important

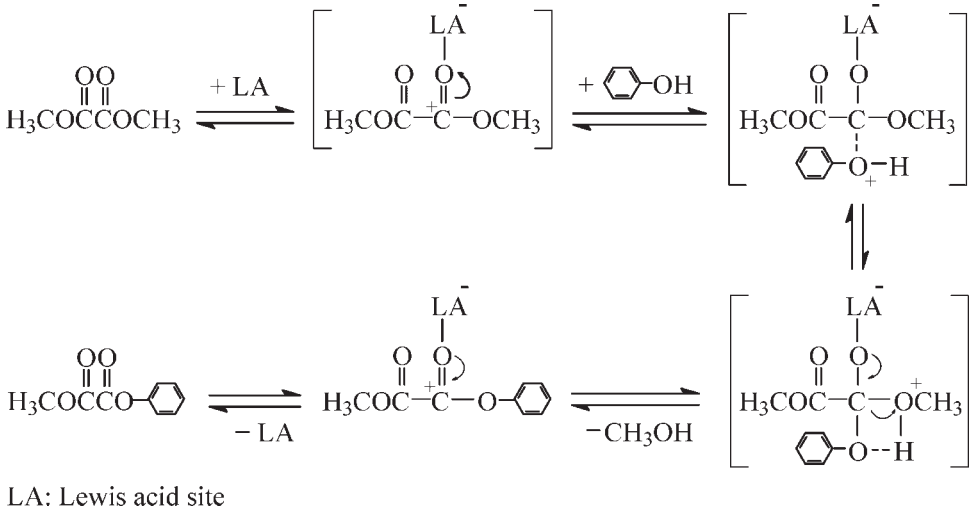

Scheme 1. A plausible reaction mechanism for transesterification of DMO with phenol.

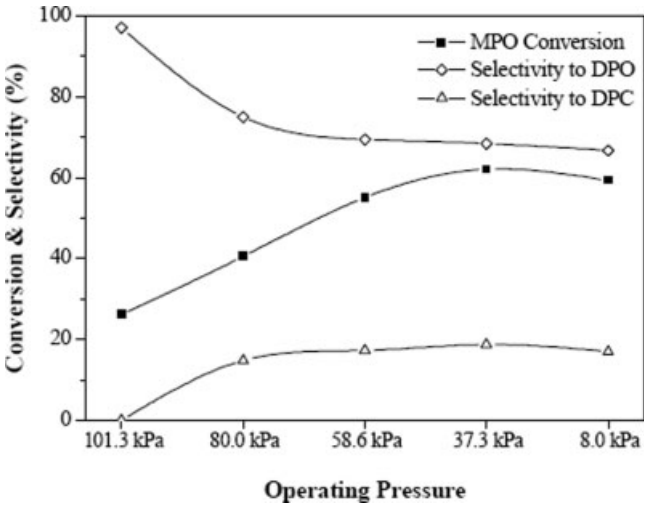

Figure 14. Influence of pressure on MPO conversion and products distribution.

role in limiting disproportionation from MPO to DPO. As shown in reaction 5, DMO is obtained as a by-product and it can be selectively removed from the reactive zone. With continuous removal of DMO, one can shift the chemical equilibrium toward the disproportionation and yield more key product DPO. Therefore, the following two steps were taken into account: the transesterification under an atmospheric pressure and the disproportionation at a low pressure. First, we carried out the transesterification at atmospheric pressure to get high DMO conversion and 99% total selectivity to MPO and DPO. Then, catalytic distillation was employed, in which heterogeneously catalyzed reaction and distillation separation occurred simultaneously. Because boiling points of phenol and DMO are lower than those of MPO and DPO, phenol and DMO could be withdrawn continually from the system at a certain pressure and temperature. Thus, the reaction equilibrium limitation in both reactions 4 and 5 was overcome and these reactions could be accelerated toward the desired direction.

The catalytic distillation experiments were operated at five different pressures and corresponding temperatures over 12 wt % TiO_2/SiO_2 catalyst. The reactants used in these experiments were the transesterification products obtained under the optimized reaction conditions. The conversion was calculated in terms of the MPO disappearance. The selectivity to DPO was determined as the amount ratio between DPO formed and MPO consumed. As illustrated in Figure 14, changing operating pressure produced a significant difference in MPO conversion and distribution of main products. MPO conversion increased drastically with a decrease in pressure from atmospheric pressure to 37.3 kPa, but decreased slightly with a further decrease to 8.0 kPa. It is noticeable that DPC was also obtained and maximized selectivity (18.7%) to DPC was achieved at a pressure of 37.3 kPa, indicating that TiO_2/SiO_2 catalyst could also catalyze the decarbonylation of DPO to produce DPC under lower pressures. These results suggest that lower pressure is apparently favorable for the disproportionation of MPO to produce DPO. However, large amounts of by-products were increasingly formed with reducing pressure. The main by-product was found to be phenyl salicylate formed from partial isomerization of DPC, as shown in reaction 8.

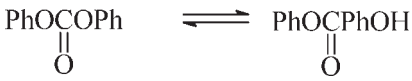

(8)

From these results, it is evident that the decrease in pressure by simple catalytic distillation significantly contributes to DPO formation. The limited data obtained from the present work cannot allow full development of an integrated model for the production of DPO, but it may provide some experimental evidences for the design of new processes in the following work. Because the principal products are DPO and DPC, the catalytic distillation can be very attractive and promising. However, high productivity of DPO as well as separation of the DPO/MPO mixture are still serious challenges. It is thus highly desirable to design an efficient catalytic distillation process for the production of high purity DPO, to simulate and optimize the practical domain of operating variables, and to search for more active solid catalysts for the disproportionation reaction. Further investigations are underway.

Conclusions

A series of TiO_2/SiO_2 catalysts with varying TiO_2 loadings (1–20 wt %) and calcination temperatures (300–800°C) have been prepared by a two-step wet impregnation method and characterized systematically by various physicochemical characterization techniques. XPS and ICP results demonstrate the monolayer dispersion capacity of TiO_2 is ~4.0 TiO_2 atoms nm^{-2} (SiO_2). XRD and Raman studies further show that titanium oxide remains highly dispersed on the silica surface at TiO_2 loadings below the monolayer dispersion capacity. The increase in TiO_2 loading or calcination temperature can result in the generation of crystalline TiO_2. FTIR of pyridine adsorption and NH_3-TPD studies show evidence suggesting the sole existence of weak Lewis acid sites on the TiO_2/SiO_2 catalysts. These results clearly reveal that there is a good correlation between the surface properties of TiO_2/SiO_2 catalysts and their catalytic behaviors in the transesterification of DMO with phenol. Monolayer-dispersed TiO_2 active centers and Lewis acidity play a crucial role in the catalytic performances, particularly regarding DMO conversion and DPO selectivity. Effects of reaction parameters such as mole ratio of reactants, catalyst amount, reaction temperature, reaction time, and catalyst recycling on the catalytic performances have been studied in the presence of the most active catalyst (12 wt % TiO_2/SiO_2 with a calcination temperature of 550°C). Based on products analysis of the transesterification over different solid acid catalysts, the Lewis acid catalyzed reaction mechanism for the transesterification of DMO with phenol was proposed. In addition, the feasibility of using catalytic distillation for the disproportionation reaction from MPO to DPO was explored at different pressures, and it was found that lower pressures favor the formation of DPO. These tentative results could help develop an integrated process of DPO synthesis for commercial applications.

Acknowledgments

The authors acknowledge the Natural Science Foundation of China (NSFC) (No.20276050), the Program of Introducing Talents of Discipline to Universities (No.B06006), and the Program for New Century Excellent Talents in University (NCET-04-0242) for their generous financial support.

Literature Cited

1. Shaikh AG, Sivaram S. Organic carbonates. *Chem Rev*. 1996;96: 951–976.
2. Fukuoka S, Kawamura M, Komiya K, Tojo M, Hachiya H, Hasegawa K, Aminaka M, Okamoto H, Fukawa I, Konno S. A novel non-phosgene polycarbonate production process using by-product CO_2 as starting material. *Green Chem.* 2003;5:497–507.
3. Gong JL, Ma XB, Wang SP. Phosgene-free approaches to catalytic synthesis of diphenyl carbonate and its intermediates. *Appl Catal A*. 2007;316:1–21.
4. Kim WB, Joshi UA, Lee JS. Making polycarbonates without employing phosgene: an overview on catalytic chemistry of intermediate and precursor syntheses for polycarbonate. *Ind Eng Chem Res*. 2004;43:1897–1914.
5. Hsu JP, Wong JJ. Kinetic modeling of melt transesterification of diphenyl carbonate and bisphenol-A. *Polymer*. 2003;44:5851–5857.
6. Ono Y. Dimethyl carbonate for environmentally benign reactions. *Pure Appl Chem*. 1996;68:367–375.
7. Vavasori A, Toniolo L. Multistep electron transfer catalytic system for the oxidative carbonylation of phenol to diphenyl carbonate. *J Mol Catal A*. 1999;139:109–119.
8. Xue W, Zhang JC, Wang YJ, Zhao XQ, Zhao Q. Oxidative carbonylation of phenol to diphenyl carbonate catalyzed by ultrafine embedded catalyst Pd-Cu-O/SiO_2. *Catal Commun*. 2005;6:431–436.
9. Tundo P, Trotta F, Molaglio G, Ligorati F. Continuous-flow processes under gas-liquid phase-transfer catalysis (GL-PTC) conditions: the reaction of dialkyl carbonates with phenols, alcohols, and mercaptans. *Ind Eng Chem Res*. 1988;27:1565–1571.
10. Niu HY, Yao J, Wang Y, Wang GY. Cp_2TiCl_2 used as a catalyst for the transesterification between dimethyl carbonate and phenol to diphenyl carbonate. *J Mol Catal A*. 2005;235:240–243.
11. Okuyama KI, Sugiyama JI, Nagahata R, Asai M, Ueda M, Takeuchi K. An environmentally benign process for aromatic polycarbonate synthesis by efficient oxidative carbonylation catalyzed by Pd-carbene complexes. *Green Chem*. 2003;5:563–566.
12. Nishihira K, Tanaka S, Harada K, Sugise R. Process for producing diaryl carbonate. U.S. Patent 5,834,615, 1998.
13. Gong JL, Ma XB, Wang SP, Liu MY, Yang X, Xu GH. Transesterification of dimethyl oxalate with phenol over MoO_3/SiO_2 catalysts. *J Mol Catal A*. 2004;207:215–220.
14. Ma XB, Gong JL, Wang SP, He F, Guo HL, Yang X, Xu GH. Characterization and reactivity of stannum modified titanium silicalite TS-1 catalysts for transesterification of dimethyl oxalate with phenol. *J Mol Catal A*. 2005;237:1–8.
15. Nishihira K, Tanaka S, Harada K, Sugise R, Shiotani A, Washio K. Process for producing a polycarbonate. U.S. Patent 5,922,827, 1999.
16. Matsuzaki T, Nakamura A. Dimethyl carbonate synthesis and other oxidative reactions using alkyl nitrites. *Catal Surv Jpn*. 1997;1:77–88.
17. Wang SP, Ma XB, Li ZH, Xu GH. Synthesis of diphenyl carbonate over Ph_4PCl. *Nat Gas Chem Eng (China)*. 2002;27:1–3.
18. Zhou WQ, Zhao XQ, Wang YJ, Zhang JY. Synthesis of diphenyl carbonate by transesterification over lead and zinc double oxide catalyst. *Appl Catal A*. 2004;260:19–24.
19. Gong JL, Ma XB, Yang X, Wang SP, Gao N, Wang DL. Comparative preparation of MoO_3/SiO_2 catalysts using conventional and slurry impregnation method and activity in transesterification of dimethy oxalate with phenol. *Catal Lett*. 2005;99:187–191.
20. Fu ZH, Ono Y. Two-step synthesis of diphenyl carbonate from dimethyl carbonate and phenol using MoO_3/SiO_2 catalysts. *J Mol Catal A*. 1997;118:293–299.
21. Wang SP, Ma XB, Guo HL, Gong JL, Yang X, Xu GH. Characterization and catalytic activity of TiO_2/SiO_2 for transesterification of dimethyl oxalate with phenol. *J Mol Catal A*. 2004;214:273–279.
22. Mei FM, Pei Z, Li GX. The transesterification of dimethyl carbonate with phenol over Mg-Al-hydrotalcite catalyst. *Org Proc Res Dev*. 2004;8:372–375.
23. Rana MS, Capitaine EMR, Leyva C, Ancheyta J. Effect of catalyst preparation and support composition on hydrodesulfurization of dibenzothiophene and Maya crude oil. *Fuel*. 2007;86:1254–1262.
24. Costa D, Arrouvel C, Breysse M, Toulhoat H, Raybaud P. Edge wetting effects of γ-Al_2O_3 and anatase-TiO_2 supports by MoS_2 and CoMoS active phases: a DFT study. *J Catal*. 2007;246:325–343.
25. Linsebigler AL, Lu G, Yates JT. Photocatalysis on TiO_2 surfaces: principles, mechanisms, and selected results. *Chem Rev*. 1995;95: 735–758.
26. Hu C, Wang YZ, Tang HX. Preparation and characterization of surface bond-conjugated TiO_2/SiO_2 and photocatalysis for azo dyes. *Appl Catal B: Environ*. 2001;30:277–285.
27. Xin BF, Jing LQ, Ren ZY, Wang BQ, Fu HG. Effects of simultaneously doped and deposited Ag on the photocatalytic activity and surface states of TiO_2. *J Phys Chem B*. 2005;109:2805–2809.
28. Zhang ZL, Zhou YS, Zhang SJ, Xu CM. Hydrodesulfurization of resid fluid catalytic cracking diesel oil over TiO_2-SiO_2 supported catalysts. *Energy Fuels*. 2006;20:2293–2298.
29. Hums E, Liebsch S, Zellbeck H. Improvement on PM reduction using a catalyst based on $V_2O_5/WO_3/TiO_2$. *Ind Eng Chem Res*. 2004;43:8001–8013.
30. Kim WB, Lee JS. Gas phase transesterification of dimethylcarbonate and phenol over supported titanium dioxide. *J Catal*. 1999;185:307–313.
31. Ma XB, Wang SP, Gong JL, Yang X, Xu GH. A comparative study of supported TiO_2 catalysts and activity in ester exchange between dimethyl oxalate and phenol. *J Mol Catal A*. 2004;222:183–187.
32. Kerkhof FPJM, Moulijn JA. Quantitative analysis of XPS intensities for supported catalysts. *J Phys Chem*. 1979;83:1612–1619.
33. Wang XY, Zhao BY, Jiang DE, Xie YC. Monolayer dispersion of MoO_3, NiO and their precursors on γ-Al_2O_3. *Appl Catal A*. 1999;188:201–209.
34. Gao X, Bare SR, Fierro JLG, Banares MA, Wachs IE. Preparation and in-situ spectroscopic characterization of molecularly dispersed titanium oxide on silica. *J Phys Chem B*. 1998;102:5653–5666.
35. Bonelli B, Cozzolino M, Tesser R, Di Serio M, Piumetti M, Garrone E, Santacesaria E. Study of the surface acidity of TiO_2/SiO_2 catalysts by means of FTIR measurements of CO and NH_3 adsorption. *J Catal*. 2007;246:293–300.
36. Gao X, Bare SR, Fierro JLG, Wachs IE. Structural characteristics and reactivity/reducibility properties of dispersed and bilayered $V_2O_5/TiO_2/SiO_2$ catalysts. *J Phys Chem B*. 1999;103:618–629.
37. Keränen J, Guimon C, Iiskola E, Auroux A, Niinistö L. Atomic layer deposition and surface characterization of highly dispersed titania/silica-supported vanadia catalysts. *Catal Today*. 2003;78:149–157.
38. Mejías JA, X Jiménez VM, Lassaletta G, Fernández A, Espinós JP, González-Elipe AR. Interpretation of the binding energy and auger parameter shifts found by XPS for TiO_2 supported on different surfaces. *J Phys Chem*. 1996;100:16255–16262.
39. Cozzolino M, Di Serio M, Tesser R, Santacesaria E. Grafting of titanium alkoxides on high-surface SiO_2 support: an advanced technique for the preparation of nanostructured TiO_2/SiO_2 catalysts. *Appl Catal A*. 2007;325:256–262.
40. Castillo R, Koch B, Ruiz P, Delmon B. Influence of the amount of titania on the texture and structure of titania supported on silica. *J Catal*. 1996;161:524–529.
41. Layman KA, Ivey MM, Hemminger JC. Pyridine adsorption and acid/base complex formation on ultrathin films of γ-Al_2O_3 on NiAl(100). *J Phys Chem B*. 2003;107:8538–8546.
42. Chen WH, Ko HH, Sakthivel A, Huang SJ, Liu SH, Lo AY, Tsai TC, Liu SB. A solid-state NMR, FT-IR, and TPD study on acid properties of sulfated and metal-promoted zirconia: influence of promoter and sulfation treatment. *Catal Today*. 2006;116:111–120.
43. Anand R, Maheswari R, Hanefeld U. Catalytic properties of the novel mesoporous aluminosilicate AlTUD-1. *J Catal*. 2006;242:82–91.

Manuscript received Jan. 22, 2008, and revision received July 9, 2008.